CHAPTER 2

Sample Synthesis and Characterization Tools

2.1 Introduction

In this chapter we have discussed the detail synthesis procedures, which have been adopted for preparation of TIs and WSMs single crystal samples. We have also discussed the working principle of different characterization tools, which is used for this thesis work for characterization of different properties of sample.

2.2 Sample Synthesis of TIs

Single crystal samples of TIs were grown by modified Bridgman techniques [42]. High purity (99.999%) precursor elements in powder form were taken in stoichiometry, mixed thoroughly then pressed in form of pallets. These pallets were then sealed in evacuate quartz ampoules. These ampoules were kept vertically inside the furnace and first heated up to 950 ^{o}C and hold at the same temperature for 24 hours, then cooled from 950 ^{o}C to 550 ^{o}C in 24 hours, then temperature retained at 550 ^{o}C for 3 days. Finally furnace was cooled to the room temperature at the ramp rate of 60 ^{o}C/h.

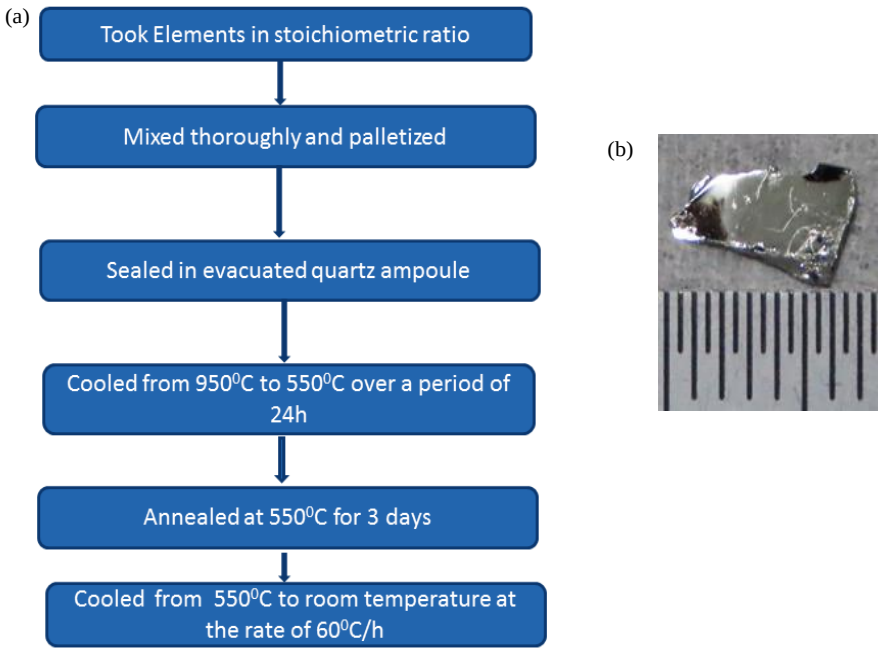

Figure 2.1: (a) Flow chart of synthesis process (b) Photograph of cleaved crystal sample.

The obtained Silver color crystals were easily cleaved along 001 crystal direction. The phase of grown single crystal samples were confirmed by X-Ray diffraction (XRD) and samples were used for other measurements. The flow chart of synthesis process and the image of cleaved single crystal sample are shown in figure 2.1.

2.3 Sample Synthesis of WSMs

The single crystal samples of WSMs were grown in two step process by adhering chemical vapor transport (CVT) technique [43]. In first step, we have kept Nb/Ta (99.99% Alfa-Aesar) and P (99.99% Alfa-Aesar) in stoichiometric amount in vacuum sealed quartz ampoule at 950 ^{o}C inside furnace for a week, and then furnace cooled slowly to the room temperature. In second step, after examining the phase purity of prepared polycrystalline samples by powder X-ray diffraction (XRD), all the polycrystalline samples were again vacuum sealed in quartz tube after loading iodine (13 mg/cm^3) as a transporting agent.

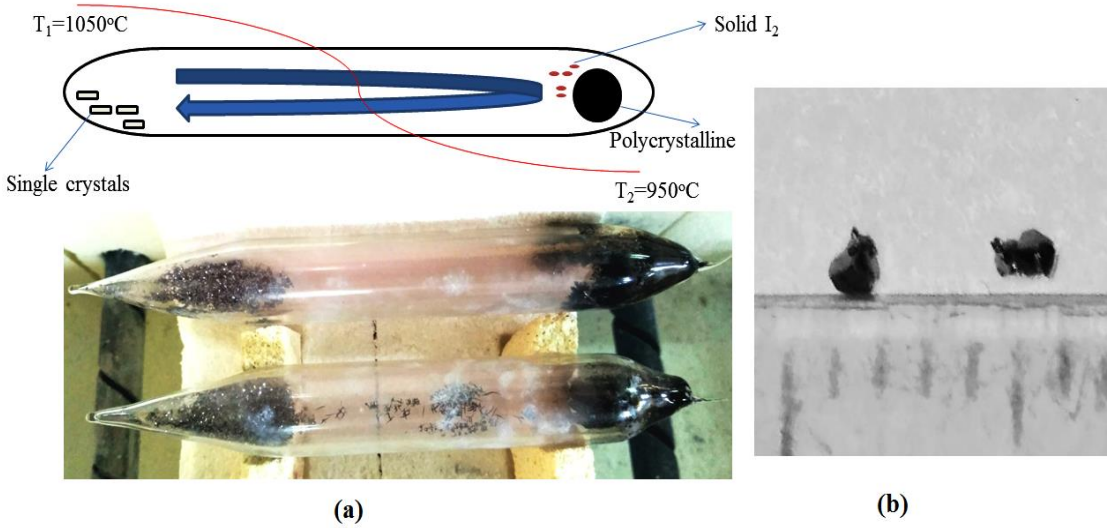

Figure 2.2: (a) Schematic of synthesis process (top) and corresponding optical image of quartz tubes placed in two zone furnace (bottom) (b) Photograph of WSM single crystal sample.

All the quartz tubes were again placed in a two zone furnace with creating a temperature gradient by maintaining one zone at 1050 ^{o}C (sink) and other zone at 950 ^{o}C (source) for three weeks. Finally, we obtained large polyhedral crystals with dimensions of up to 1.0 mm, as displayed in figure 2.2.

2.4 Experimental Characterization Tools

2.4.1 X-Ray Diffraction (XRD)

Phase confirmation for the synthesized samples was carried out by XRD. When a monochromatic beam of X-ray is incident on the sample, the incident X-ray photons are interact to the electrons of an atom in the sample as a result some of the photons are diffracted away from their original incident direction. Diffraction is the phenomenon in which the electromagnetic wave bend form an obstacle if the size of obstacle is comparable to wavelength of wave. An inter-atomic distance in crystalline materials lies in the range of 1 to 10 Å which is the same order of X-ray wavelength. There are only certain directions in which diffracted wave interfere constructively and interference peaks are observed for a particular crystalline solid at particular angles. Atoms are arranged periodically in the crystals, if the interference occurred by diffracted waves from the atomic planes satisfy Bragg's condition then it gives the X-ray diffraction pattern of a given material by measuring the intensity of diffracted waves with variation of the X-ray incident angle. XRD technique is not only identify the phase of synthesized sample, but also provides the information of crystal structure and the dimension of unit cell.

A relation between inter-atomic distance 'd', wavelength of the incident beam 'λ' and angle of incident beam 'θ' has been given by W. Lawrence Bragg and William H. Bragg, known as Bragg's law [44]. Bragg's relation stated as

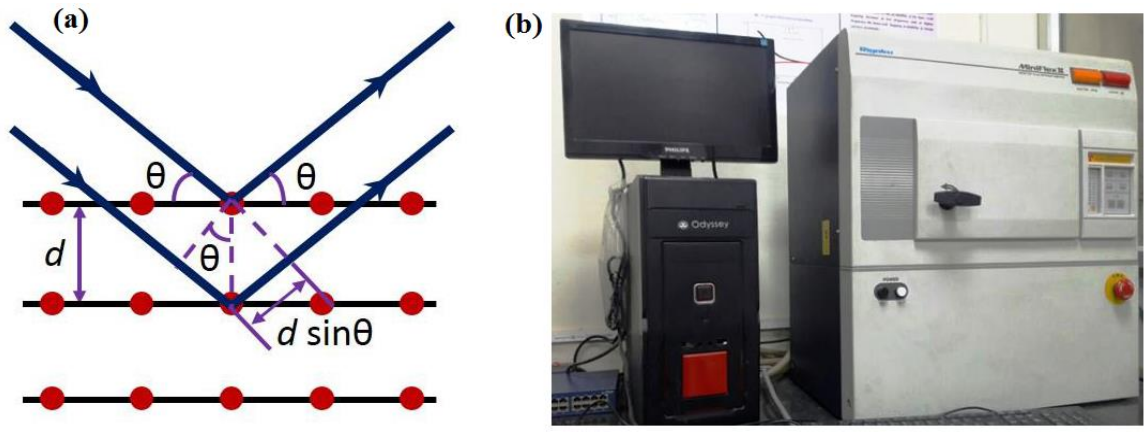

Figure 2.3: (a) Photographic demonstration of Bragg's law (b) Actual photograph of Rigaku Mini Flex II DESKTOP X-ray diffractometer set up.

$$2d \sin\theta = n\lambda \tag{2.1}$$

Where n is integer, representing the order of diffraction.

The intensity of diffracted X-ray is recorded as a function of the Bragg angle 2θ. The Rigaku-Miniflex II DESKTOP powder X-ray diffractometer as shown in figure 2.3 was used to record the intensity vs 2θ data. This diffractometer has a monochromatic X-ray source with CuK_α radiation (λ=1.5418 Å) at 30 kV and 15 mA.

2.4.2 Laue Diffraction Pattern

The Laue diffraction analysis was carried out on cleaved single crystals. When a beam of polychromatic X-ray radiation is incident on an immovable single crystal, since Bragg's angle θ is constant for each set of planes in the crystal therefore each set diffracts a distinct wavelength which fulfills the Bragg's condition for the particular values of d and θ. There are two different measurement geometries in which Laue diffraction can be accomplished based on the relative positions of the X-ray source and sample (1) the transmission geometry (2) back-reflection geometry. The schematics of both the geometries are shown in figure 2.4 (a, b).

In both the geometries, sample is placed in such a way that X-rays incident normally on the sample. In the transmission geometry, the X-ray beam incident on the sample gets partially

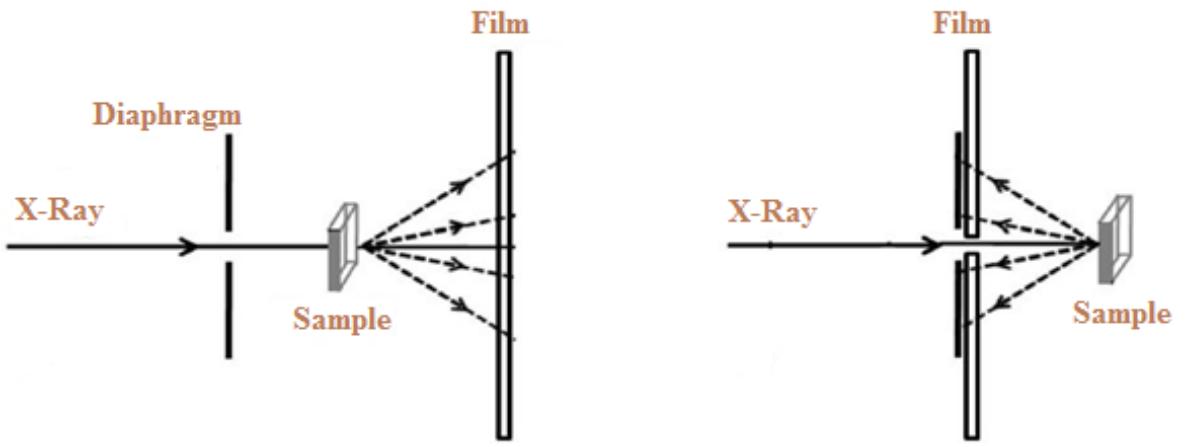

Figure 2.4: Schematic of (a) Transmission Laue diffraction geometry (b) Back-reflection Laue diffraction geometry.

transmitted through the sample and recorded on the photographic film. Whereas, in the back-reflection geometry, the photographic film is placed somewhere in the middle of the X-ray source and sample. The backward diffracted beams from the sample are recorded on photographic film. In both these geometries, the diffracted beams form an array of spots for a single crystal sample.

2.4.3 Transport Properties Measurements

2.4.3.1 Electric Resistivity (ρ_{xx})

Resistivity of the synthesized single crystal samples was recorded using Quantum Design Physical Property Measurement system (QD-PPMS) by adopting four-probe method. When electrons travel through the crystal, they feel the resistance in their motion. To move the electrons against this resistance a potential difference is needed to apply across the crystal. According to Ohm's law, if current I flow through the crystal that have resistance R, then voltage V will drop against this resistance through the crystal from equation V = IR. The quantity that characterizes the material is resistivity (ρ_{xx}). The resistivity of particular material depends on the synthesis process. The resistivity of a crystal is inversely proportional to the

length l between two voltage probes and proportional to the cross-section area A. Mathematically, it is expressed as

$$\rho_{xx} = \frac{RA}{l} \tag{2.2}$$

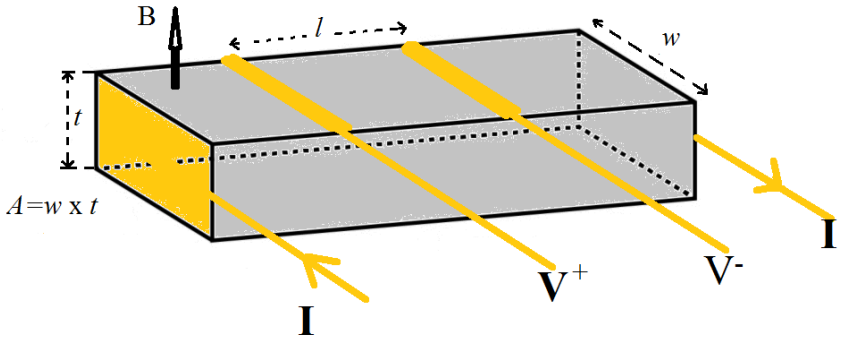

Figure 2.5: Schematic of four-probe measurement geometry.

The resistivity measurements were carried out on a uniform rectangular single crystal sample by employing a conventional four-probe technique between 2 K and 300 K with (MR) and without (ordinary resistivity) applying external magnetic field B normal to the surface of sample as shown in figure 2.5.

2.4.3.2 Hall Resistivity (ρ_{xy})

Hall resistivity measurement was also accomplished by using Quantum Design Physical Property Measurement system (QD-PPMS) by changing the connection geometry as displayed in figure 2.6. In this case the voltage drop was measured across the opposite surfaces of the sample perpendicular to both current (I) and external applied magnetic field (B). When a particle of charge q moves perpendicular to B in a current carrying conductor, a Lorentz force $\mathbf{F} = q\boldsymbol{v}\times\boldsymbol{B}$ is developed on the charge perpendicular to both the direction of the particle motion and the field. Therefore, by applying a fixed longitudinal current I across a sample, the transverse voltage or Hall voltage V_H is measured as mentioned in section 1.5.1. The graph between measured Hall resistivity ρ_{xy} versus applied magnetic

field gives the accurate value of Hall coefficient (R_H =1/nq). A linear variation of ρ_{xy} as a function of field is yielded and the value of R_H is determined from the slope of this linear line. A negative value of R_H indicates n-type nature of charge carriers in a sample while a positive value of R_H suggests p-type nature of charge carriers. The voltage difference measured between two opposite surfaces provides the value of Hall voltage V_H and the Hall resistivity can be obtained as,

$$\rho_{xy} = \frac{V_H A}{Il} \tag{2.3}$$

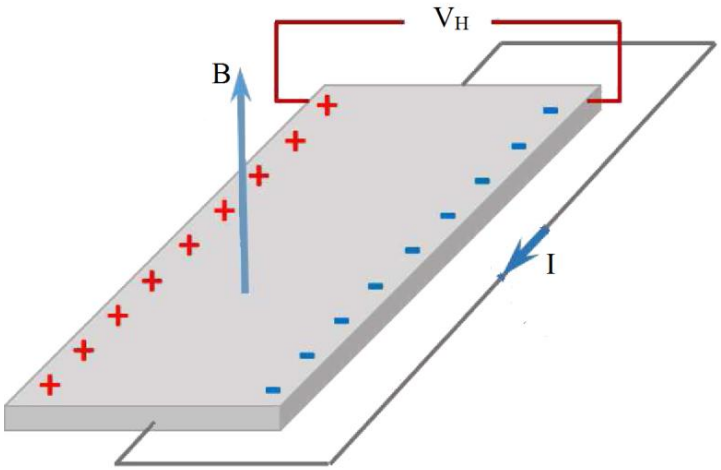

Figure 2.6: Schematic diagram for Hall effect measurement.

2.4.3.3 Thermoelectric Measurement

The Seebeck coefficient (*S*) was determine by homemade setup in which sample was sandwiched in between two copper blocks. The sample holder assembly was mounted on the close cycle refrigerator (CCR) which was able to cool up to 20 K from room temperature in controlled manner. The temperature difference across the sample was maintained at 2 K with the help of T-type thermocouple by placing two heater coils at both ends of two copper blocks. The voltage difference (ΔV) between the cold end and the hot

end was measured with the help of keithley 2182A nano-voltmeter from low temperature to the room temperature. The sample holder assembly is illustrated in figure 2.7.

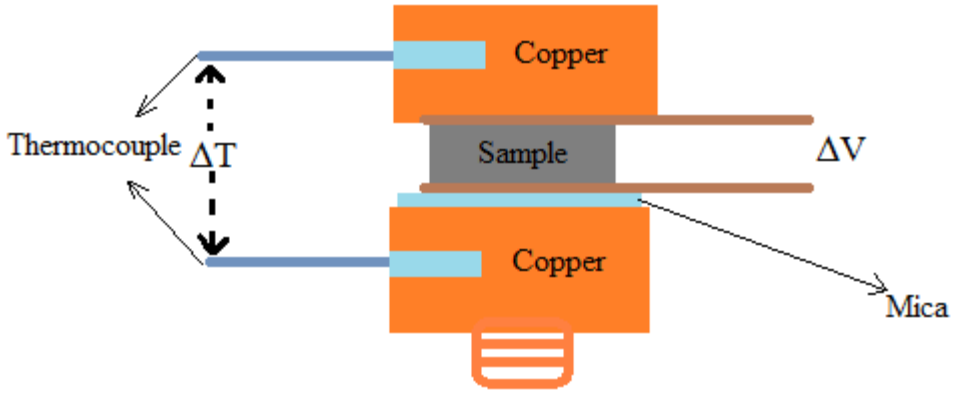

Figure 2.7: Schematic diagram of sample holder for thermoelectric measurement.

Temperature difference at the both ends of the sample creates a temperature gradient; consequently, there is diffusion of charge carriers from hot end to the cold end, which generates a thermal current. Seebeck coefficient (*S*) is the ratio of magnitude of an induced thermoelectric voltage ΔV with respect to the temperature difference ΔT across the sample, given as

$$S = \frac{\Delta V}{\Delta T} \tag{2.4}$$

Where, *S* is measured in μV/K and its slope gives the nature of transport carrier. A negative slope indicates n-type nature of transport carriers in a sample while the positive slope suggests p-type nature of transport carriers.

2.4.4 Magnetic Property Measurement System (MPMS)

Quantum Design (QD) MPMS is designed to examine the magnetic properties of small samples over a wide range of magnetic fields and temperatures. This device is able to measure a very small change in magnetic field with enormous precision. It is controlled by

several electronic controllers and provides data collection by a computer. Magnetic measurements are performed by extremely sensitive Superconducting Quantum Interference Device (SQUID). Thus, the MPMS is often called SQUID magnetometer. The QD-MPMS is most widely used to measure the magnetic property through vibrating sample magnetometer (VSM) mode. A solenoid of superconducting wire (Superconducting magnet) is used in MPMS to produce a magnetic field up to ± 7 Tesla (± 70 kOe). The superconducting magnet and SQUID detector both are cooled by liquid helium. Sample chamber is cooled by the combination of both liquid nitrogen and liquid helium. MPMS covers the large temperature range measurement from 2 K–480 K with magnetization measurement sensitivity of 5×10^{-8} emu. In SQUID VSM, sample vibrates sinusoidally with the frequency ω about the center of the detection coils, where the signal picks as a function of position of the sample Z (t).Therefore, the expression for generated SQUID signal V (t) as a function of time t can be given as,

$$Z(t) = \text{Sin}\,(\omega t) \tag{2.5}$$

And

$$V(t) = A\,Z^2(t) \tag{2.6}$$

$$V(t) = AB^2\sin^2(\omega t) \tag{2.7}$$

Here, A is a scaling factor relating to the magnetic moment of the sample and B is the sample vibration amplitude. In this system, the SQUID works as extremely sensitive current to voltage converter and inductively coupled with detection coil. Basically, the SQUID functioning is based on Josephson tunneling effect and flux quantization in superconducting

ring. Due to vibration of magnetic sample through the coils, the coils generate the current in the response of the disturbance in local magnetic field. The SQUID feedback nulls the current in the pickup coils, so basically there is no flow of current in them; hence the SQUID voltage corresponds to the feedback current gives the value of sample magnetization. All the magnetic measurements of present thesis are performed by QD-MPMS-SQUID-VSM which is shown in figure 2.8.

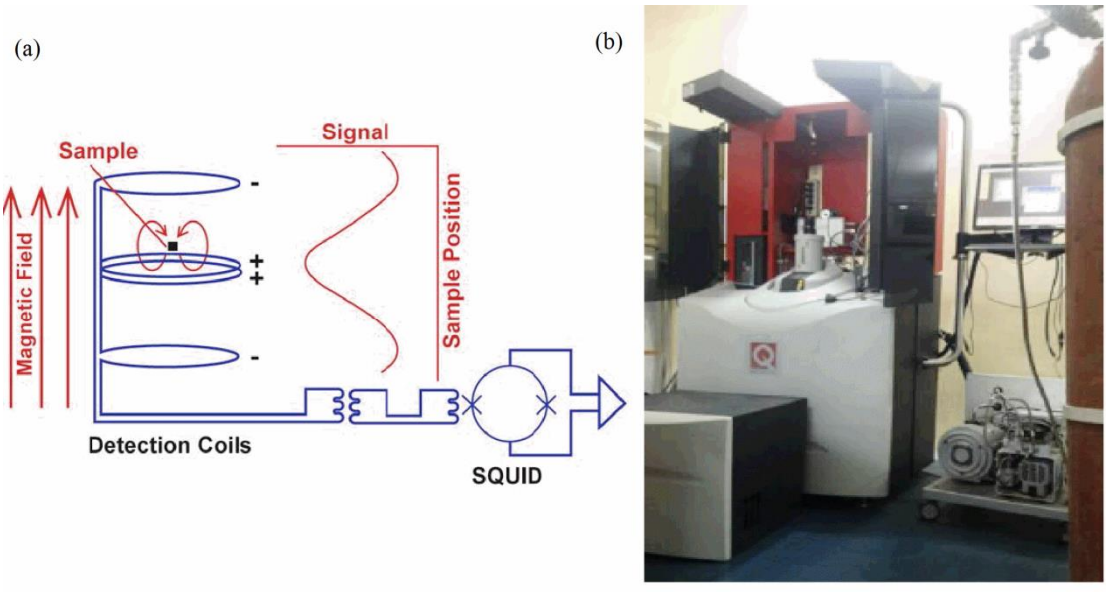

Figure 2.8: (a) Schematic diagram of SQUID-VSM detection system [45] (b) Photograph of actual QD-MPMS measurement system.

2.4.5 Photoemission Spectroscopy

History of photoemission commences with the well-known experiment demonstrated by Heinrich Hertz in 1887[46]. He observed that if an ultraviolet light illuminated on a material surface a negative charge can be drew out from its surface. Thereafter, in 1905 Albert Einstein established the quantum nature of light and explained the photoemission process[47]. Nowadays, photoelectron spectroscopy is one of the most useful tools to understand the electronic structure of a material. The microscopic electron's dynamics near the E_F is the origin of most of the macroscopic properties exhibited by materials. Therefore,

very high resolution analyzers are required to analyze these very low energy electronic states. In mid 1990s Scienta has developed an electron analyzer with energy resolution 20-40 meV, which has now improved to 5 meV. In recent years, a vacuum ultraviolet laser based photoemission spectrometer has also been developed with very fine resolution. These technical developments provide the experimental confirmation of many peculiar properties, such as TSS, topological Fermi arcs etc.

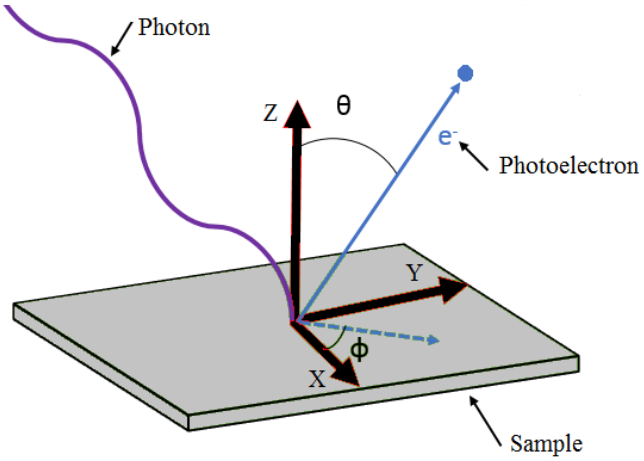

Figure 2.9: Illustrational of photoemission process.

Photoemission processes are based on the photoelectric effect as illustrated in figure 2.9. When a photon of energy E = hν incident on the surface of a material and the photon energy is high enough then it can extracted an electron from bound state of material. The extracted electron is called a photoelectron and its kinetic energy (E_{KE}) can be measured by using an analyzer. The E_{KE} of the photoelectron is given as,

$$E_{KE} = h\nu - (E_{BE} + W_{\varphi}) \tag{2.8}$$

Where, E_{BE} is the binding energy of electron and W_{φ} is the work function of material. The momentum (k) of the photoelectron can also be estimated from the E_{KE} as,

$$\boldsymbol{k} = \frac{\sqrt{2m_e E_{KE}}}{\hbar} \tag{2.9}$$

Based on the frequency of incident photons and phtoelectron analyzers, two photoemission spectroscopy have been widly used by resercher to charaterized the material.

2.4.5.1 X- Ray Photoemission Spectroscopy (XPS)

XPS is a quantitative spectroscopic technique to identify of oxidation state, elemental composition and empirical formula within a material.

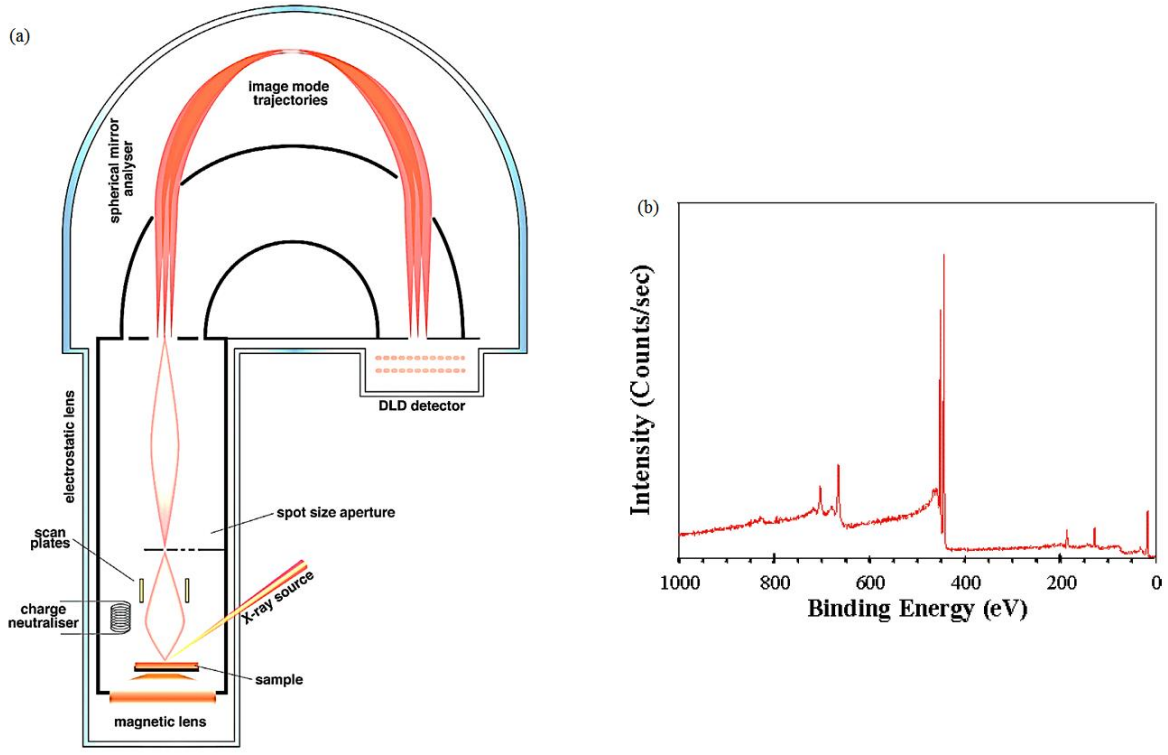

Figure 2.10: (a) Schematic diagram of XPS [48] (b) Typical XPS spectrum from a cleaved sample surface.

The surface of the materials is irradiated by a beam of X-rays and simultaneously the kinetic energy of electrons librated from the top 1 to 10 nm surface layers of the material is measured. Therefore, it is a surface sensitive technique and it can probe the surface ligand structure of any particles size. An Ultra-high vacuum (UHV), typically a oreder of $\sim 10^{-10}$ torr is required for measurement. Such a high order vacuum not only expedites the movement of the photoelectrons to the analyzer but also reduces the rate of re-

contamination of a newly cleaned sample. When sample surface is illuminated by monochromatic low energy X-rays (~1.5 keV) source then the core level electrons are ejected from the surface of sample as a consequence of photoemission process. In XPS, a high-resolution spectrometer is used to measure the energy spectrum of the ejected photoelectrons. XPS spectra is plotted as a function of binding energy of detected electron displayed on X-axis and number of detected electrons (counts per second) are shown on Y-axis. Each emitted photoelectron exhibits a individual set of XPS peaks at characteristic binding energy values. Thus, from this data, we can directly recognize perticular element that presents in or on the surface of the material that is being analyzed. The schematic diagram and a typical XPS spactrum is shown in figure 2.10.

2.4.5.2 Angle-resolved Photoemission Spectroscopy (ARPES)

ARPES is a useful technique that provides direct visualization of the electronic structure in the materials. Its working is also based on the famous photoelectric effect. According to the information of interest, the energy or momentum of photoemitted electrons from the material can be investigated. This is facilitated by the conservation of energy and momentum in the photoemission process. Similar to the XPS, the ARPES experiment is also accomplished in a UHV environment when a highly intense monochromatic incident photon beam generally emanates from a synchrotron source. The bulk electronic band structure along with TSS can be clearly seen from ARPES measurement for TIs. Hence, one can clearly distinguished the conduction band, valance band and TSS as well as the presence of bulk band gap in the materials. So, ARPES is a useful tool for inspecting the effect of magnetic doping on the TSS in TIs. Because, TSS in TIs are protected by TRS, hence these are unaffected by nonmagnetic impurities and there is no band gap at DP, but contrastingly, the doping of magnetic impurity breaks the TRS, hence creates a gap opening

at the DP. From the conservation of energy (eq. 2.8) and momentum (eq. 2.9) of photoemitted electron, and by associating the momentum of the ejected electron to its detected angle, we can determine the wavenumber of the photoemitted electron as,

$$k_x = \frac{\sqrt{2m_e E_{KE}}}{\hbar} \sin\theta \ \sin\phi \tag{2.10}$$

$$k_y = \frac{\sqrt{2m_e E_{KE}}}{\hbar} \sin\theta \ \cos\phi \tag{2.11}$$

$$k_z = \frac{\sqrt{2m_e E_{KE}}}{\hbar} \cos\theta \tag{2.12}$$

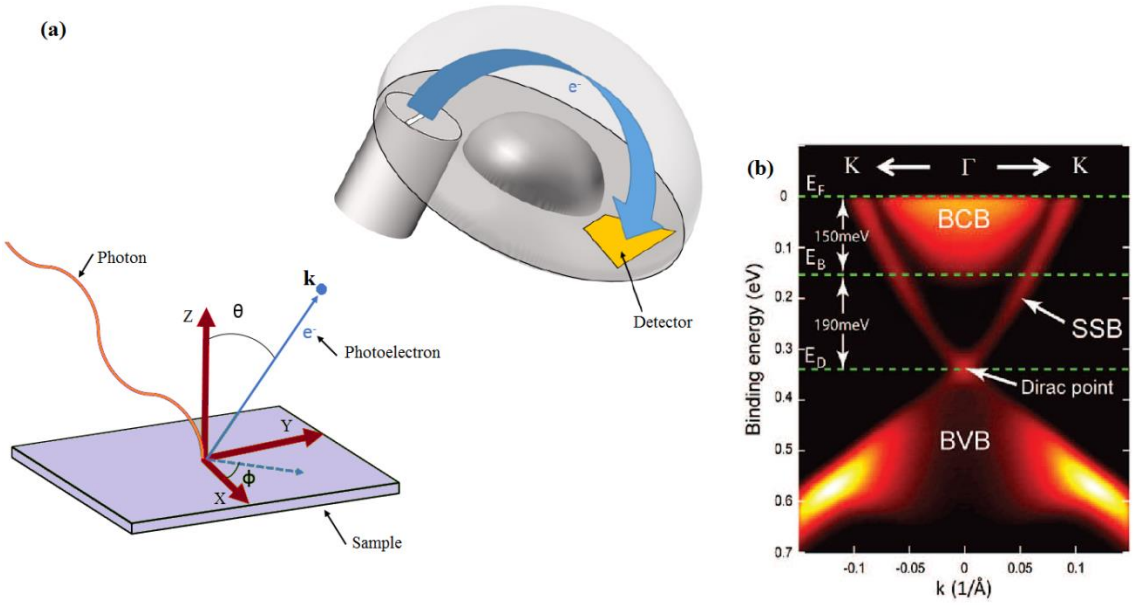

Figure 2.11: (a) Schematic of ARPES measurement setup (b) Shows ARPES spectra of pure Bi_2Se_3 TI [30].

Therefore, by combining these momentums with the energy, one can able to fully map the E(k) dispersion relation of the electrons in the Brillouin zone. All the compounds are not appropriate for ARPES measurement as it require a fresh and uniform surface that is generally achieved by cleaving of single crystals. Hence, if single crystals are not available,

and if the single crystals are very hard to cleave the ARPES measurement becomes difficult. Figure 2.11 (b) displays the ARPES spectra of pure Bi_2Se_3 TI, the gap between the bulk valance band (BVB) and bulk conduction band (BCB) is 190 meV and location of the DP is 340 meV below the E_F, it bridges the upper and lower part of Dirac cones. Nearly linear Dirac-like surface states bands (SSB) or TSS are clearly visible from the spectra.

2.5 Theoretical Band Structure Calculations

For better understanding the electronic band structure and to support the experimental results, we have performed the theoretical calculations for our materials. All the calculations are executed within the context of density functional theory (DFT) using Vienna ab-initio simulation package (VASP) and WIEN2k package. The Perdew-Bruke-Ernzerhof generalized gradient approximation (PBE-GGA) is adapted as exchange-correlation functional and the core and valence interaction effects are incorporated in terms of projector-augmented-wave (PAW) method. Over the past few years DFT has emerged as the most successful and enormously employed methodology to describe the properties of condensed matter systems. The basic motive to perform the DFT calculations is to obtain deeper insight on our experimental results.